DOR:

Research Paper

Analyzing Thermomechanical Characteristics: A Comparative Study of Stationary Shoulder FSW and Conventional FSW

Mostafa Akbari[1*], Ezatollah Hassanzadeh[1], Yaghoub Dadgar Asl[1], Milad Esfandiar[1], Hossein Rahimi Asiabaraki[1]

[1]Department of Mechanical Engineering, Technical and Vocational University (TVU), Tehran, Iran

[*]Email of Corresponding Author: mo-akbari@tvu.ac.ir

Received: November 30, 2023; Accepted: January 25, 2023

Abstract

Friction Stir Welding (FSW) has significantly transformed the metal joining industry, and an innovative variation known as stationary shoulder FSW has emerged. This study aimed to compare various aspects, including force, temperature, and strain, between conventional friction stir welding (CFSW) and stationary shoulder friction stir welding (SSFSW). To accomplish this, the finite element method was employed, utilizing the lagrangian technique to model the welding process. The findings revealed that in SSFSW, the highest temperature was observed in the vicinity of the rotating pin. This was attributed to the absence of a rotating shoulder in SSFSW, which played a major role in heat generation during welding. The upper-temperature limit in the welding cross-section has been decreased from 350 degrees Celsius in the case of CFSW to 200 degrees Celsius for SSFSW. Moreover, the longitudinal forces on the tool in SSFSW were significantly higher compared to CFSW. During the advancing stage of FSW, the applied force typically falls within the range of 2 to 3 kN. In contrast, in SSFSW, during the same advancing stage, the force undergoes a significant increase and ranges between 15 to 20 kN. In the CFSW process, the strain-affected area usually forms a basin-shaped pattern. However, in the SSFSW process, the strain distribution is confined within the range of the tool pin.

Keywords

FSW, SSFSW, Force, Strain, Temperature

1. Introduction

Friction stir welding has emerged as a highly promising solid-state joining technique since its invention in the early 1990s [1, 2]. Unlike traditional fusion welding methods, FSW utilizes a non-consumable rotating tool to generate frictional heat and plasticize the material, forming a high-quality weld joint [3, 4]. This innovative process has found extensive applications in various industries, including aerospace, automotive, and shipbuilding, due to its ability to produce defect-free welds with superior mechanical properties. FSW offers several advantages over conventional welding methods, such as reduced distortion, improved fatigue performance, and enhanced joint integrity [5, 6]. As a result, it has garnered significant attention from researchers and industry professionals alike.

The field of friction stir welding has witnessed significant advancements in recent years, leading to the development of innovative techniques aimed at enhancing weld quality and process efficiency [7-9]. One such technique is Stationary Shoulder Friction Stir Welding (SSFSW), which deviates from the conventional FSW method by incorporating a stationary shoulder during the welding process [10, 11]. The stationary shoulder technique introduces a unique approach by eliminating the rotational motion of the shoulder, resulting in distinctive thermomechanical characteristics during the welding process [12,13]. This novel technique has gained attention due to its potential to improve weld properties, including joint strength, microstructural refinement, and defect reduction.

Despite the significant attention received by researchers and application engineers, the practical utilization of the SSFSW method in production settings remains relatively uncommon. One contributing factor to this limited adoption is the lack of comprehensive studies investigating the differences in thermal history and strain patterns between weldments produced through CFSW and SSFSW. While FSW has undergone extensive scrutiny and implementation across various industries, SSFSW possesses unique characteristics and advantages that have yet to be fully explored and comprehended.

Comprehensive studies comparing FSW and SSFSW are of utmost importance to address the existing knowledge gap and promote the broader implementation of SSFSW in industrial production. By acquiring a profound understanding of the distinctive thermal and mechanical properties exhibited by SSFSW weldments, manufacturers can effectively assess and embrace this advanced welding technique, thereby fostering enhanced productivity, bolstered structural integrity, and heightened efficiency across diverse industries.

This article presents a comprehensive analysis and comparison of the thermomechanical behavior between SSFSW and CFSW. The aim is to shed light on the advantages and limitations of this emerging welding technique. To begin, both FSW and SSFSW processes are modeled using Deform-3D^{TM} software. The temperature distribution within the welding zone is then investigated and compared between the two processes. Following that, the strain distribution in the cross-section of the welded samples is examined for both processes. Finally, the focus shifts to the examination of welding forces, which are crucial parameters throughout the tool's lifespan.

2. Simulation details

To conduct a comprehensive investigation into the temperature distribution, strain patterns, and forces involved in FSW and SSFSW, the powerful simulation software Deform-3D^{TM} was employed as a valuable tool [14]. In this study, a Lagrangian formulation was adopted as the numerical simulation approach, ensuring accurate modeling of the dynamic aspects of the welding process. The joints were created using traverse and tool rotational speeds of 60 mm/min and 900 rpm, respectively, with aluminum profiles being joined in a butt configuration, as depicted in Figure 1. Both FSW and SSFSW techniques were employed to accomplish the welds, facilitating a comprehensive comparative analysis of their respective characteristics and performance.

Figure 1. Schematic representation of FSW & SSFSW

For the FSW process, a specialized tool configuration was utilized. The FSW tool consisted of a shoulder with a diameter of 18 mm.

Additionally, it incorporated a cylindrical pin design with a diameter of 4 mm. In the case of the SSFSW technique, the tool configuration included a stationary shoulder with a diameter of 18 mm and a pin diameter of 4 mm.

The tool employed in the simulation was treated as a rigid body and discretized with tetrahedral elements to capture its intricate behavior. In addition, to accurately represent the workpiece and its response to the FSW tool, the workpiece was divided into multiple zones and meshed using different element sizes [15, 16]. Specifically, smaller elements with a mean length of 0.8 mm were concentrated in the vicinity of the FSW tool to improve the simulation accuracy, as depicted in Figure 2.

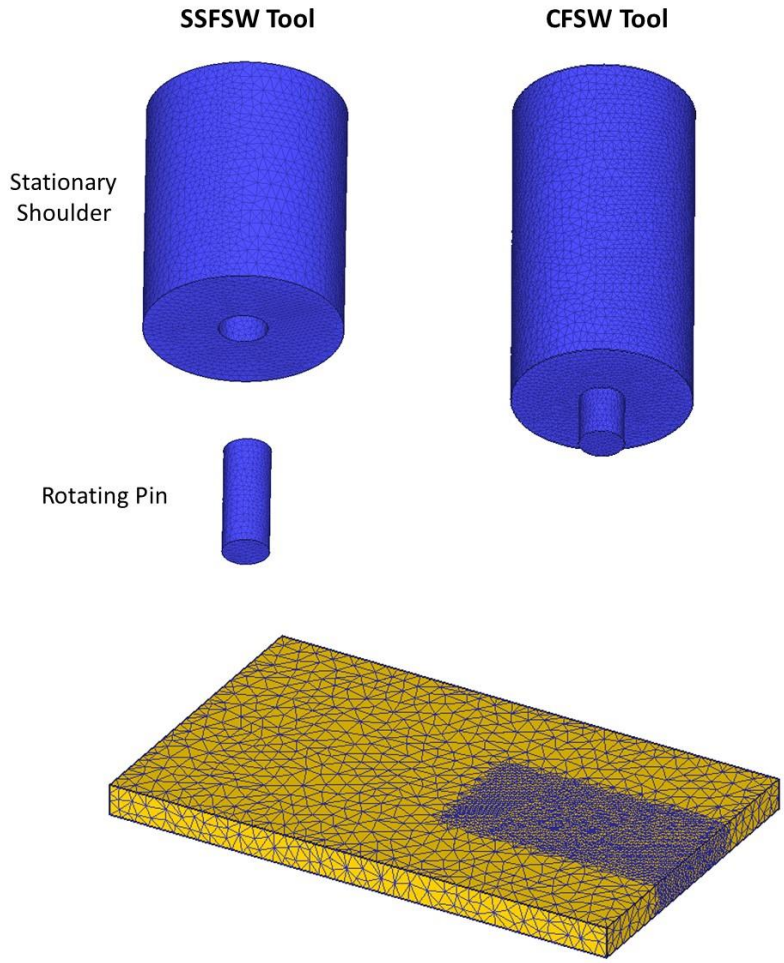

Figure 2. Illustration of the workpiece and the FSP tool.

The FSW was performed on A356 aluminum with a thickness of 10 mm, and the chemical compositions are given in Table 1.

Table 1. Chemical composition of as-cast A356 aluminum plates (wt%).

Si	Fe	Mn	Cu	Zn	Ti	Mg
7	0.31	0.1	0.2	0.1	0.25	0.3

The flow stress of A356 aluminum alloy is given as a function of strain rate, plastic strain, and temperature [17, 18]:

$$\bar{\sigma} = \bar{\sigma}(\bar{\varepsilon}, \dot{\bar{\varepsilon}}, T) \quad (1)$$

Where $\bar{\sigma}$ represents the flow stress, $\bar{\varepsilon}$ represents the plastic strain, $\dot{\bar{\varepsilon}}$ represents the strain rate, and T is the temperature.

Constant shear friction is utilized to model friction between the tool and workpiece, mainly in this study. In the constant shear model, the frictional force could be calculated as follows [18]:

$$f = mk \quad (2)$$

Where *f*, *k*, and *m* represent the frictional stress at the tool-workpiece interface, the shear yield stress, and the shear friction factor.

In this study, the convective boundary condition for all weldment surfaces is defined as [15]:

$$k\frac{\partial T}{\partial n} = h(T - T_{amb}) \tag{3}$$

Where *h* represents the convection coefficient, T_{amb} is the ambient temperature, and *n* is the boundary's normal vector. The convection coefficient for the material surfaces displayed to the environment is considered 20 W/(m^2.ºC). Moreover, the thermal properties of the H13 steel tool and A356 samples are summarized in Table 2.

Table 2. Thermal properties of the A356 aluminum alloy and H13 FSW tool

Property	A356	FSW Tool
Heat capacity (N/mm2◦C)	2.57	4.5
Conductivity (W/m◦C)	117	24.5
Heat transfer coefficient between tool and billet (N/◦C s mm2)	11	11
Heat transfer coefficient between backing plate and billet (N/ C s mm)	5	-

3. Result and discussion

3.1 Temperature comparison between FSW and SSFSW

In FSW, a rotating tool with a specially designed shoulder and pin is used to plunge into the joint interface, generating heat through frictional forces and plastic deformation. The primary heat source is the frictional contact between the shoulder and the workpiece, resulting in localized heating. The temperature distribution during FSW is typically non-uniform, with the highest temperatures occurring in the weld stir zone and gradually decreasing towards the periphery (Figure 3). The heat-affected zone (HAZ) adjacent to the SZ experiences varying levels of thermal exposure, which may influence the material's microstructure and mechanical properties.

SSFSW introduces a stationary shoulder instead of the rotating shoulder used in FSW. The stationary shoulder remains in contact with the workpiece throughout the welding process, acting as a heat sink. This modification alters the temperature distribution in the weld region. The presence of the stationary shoulder leads to reduced heat generation and improved heat dissipation, resulting in a more uniform temperature profile (Figure 3). In CFSW, the highest temperature is seen near the surface of the samples and under the shoulder of the tool. This distribution is due to the presence of the rotating shoulder, which has the greatest effect on the generation of frictional heat. In SSFSW, the temperature distribution is completely different from CFSW, so the highest temperature is seen in the vicinity of the rotating pin. Due to the absence of a rotating shoulder like CFSW, the shoulder does not play a role in generating heat during welding.

Moreover, by absorbing and dissipating a significant amount of heat, the stationary shoulder reduces the peak temperatures in the weld area and its surrounding regions. As can be seen in Figure 3, the maximum temperature in the welding cross-section has been reduced from 350 degrees for CFSW to 200 degrees Celsius for SSFSW.

The introduction of the stationary shoulder in SSFSW contributes to a narrower and better-defined HAZ compared to FSW. The reduced thermal exposure in the HAZ minimizes the potential for adverse metallurgical changes, such as grain growth, hardness variations, and residual stresses. This allows for improved joint quality, enhanced mechanical properties, and better overall weld performance.

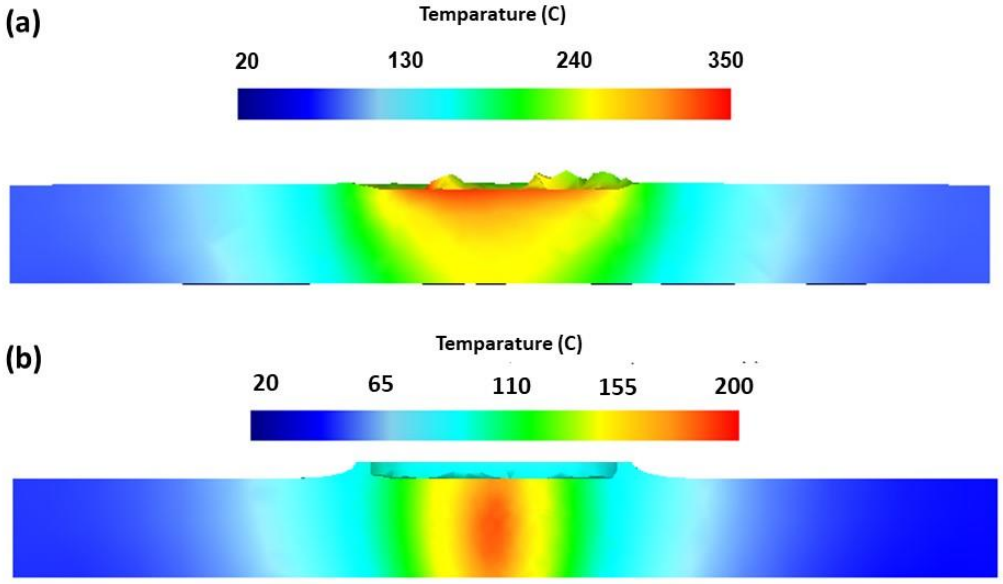

Figure 3. Temperature variation of the sample produced by a) FSW b) SSFSW

3.2 Force comparison between FSW and SSFSW

The force exerted on the tool during the FSW/ SSFSW process plays a crucial role in determining its wear characteristics and overall lifespan [19, 20]. The tool encounters different forces, including lateral, longitudinal, and axial forces, throughout the process. An axial force is applied during tool penetration into the specimen in FSW/ SSFSW, causing an upward-lifting effect on the tool. This force arises from the resistance encountered by the tool as it interacts with the workpiece material. Various factors, such as material properties, process parameters, and the design of the FSW machine, influence the magnitude of this force [21]. In certain FSW/ SSFSW machines, the axial force is actively controlled to maintain a consistent level throughout the process [22]. This control ensures a steady tool penetration rate and minimizes variations in force. Conversely, in some FSW setups, the process relies on controlling the tool's vertical position, which unintentionally leads to changes in the applied force during the process. These fluctuations in force during the FSW process can impact the tool's performance and wear characteristics. Figure 4 illustrates the axial force characteristics of FSW and SSFSW. In FSW, a rotating tool is inserted into the samples. During the plunging stage, when the tool pin makes contact with the workpiece surface, the axial force experiences a significant increase due to a combination of material softening and work hardening. The plunging stage can be divided into two phases: when the pin penetrates the workpiece surface and when the tool shoulder reaches the surface of the sample. The maximum axial force is observed when the shoulder fully penetrates the sample.

In SSFSW, axial forces act on both the pin and shoulder of the tool. Initially, during the tool's penetration, the force is applied solely to the tool pin. As the shoulder of the tool comes into contact with the workpiece, the axial force gradually increases and reaches its peak at the end of the tool's penetration stage. Subsequently, the axial force reduces and fluctuates within a specific range. In comparison to conventional FSW, the axial force exerted on the tool during tool advancement is significantly higher in SSFSW. This disparity arises due to the heat generated by the shoulder, which raises the temperature of the material in the welding zone in CFSW. The shoulder's frictional heat production causes the material to soften, thereby reducing its resistance to the tool's movement and decreasing the force exerted on the tool.

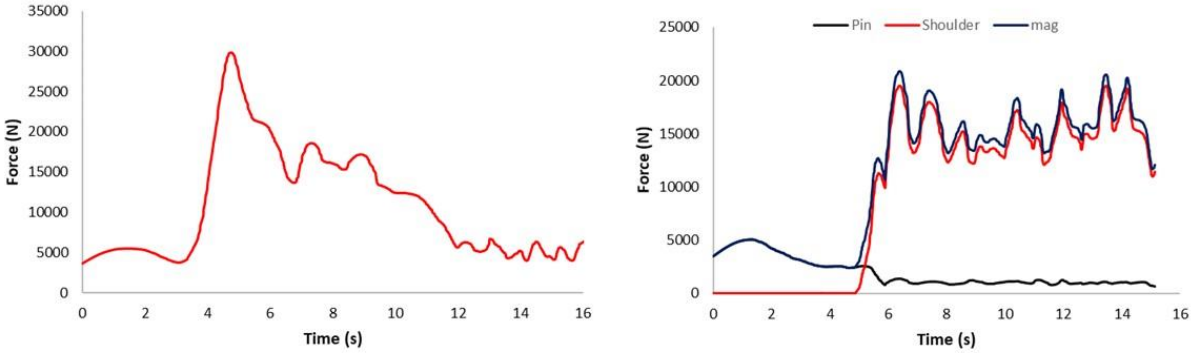

Figure 4: Comparison of axial force between FSW and SSFSW

Figure 5 provides a visual representation of the longitudinal forces acting on the tool in two welding processes. Notably, the longitudinal forces experienced by the tool in SSFSW are approximately ten times greater than those in CFSW.

In SSFSW, the majority of the axial force is applied to the shoulder of the tool. This indicates that the shoulder bears the brunt of the force during the welding process. The rotational movement of the tool pin in SSFSW generates frictional heat as it rotates around itself. This heat generation causes the material to soften, resulting in reduced resistance against the pin. Consequently, the force exerted on the pin decreases. Figure 3 supports this observation by indicating that the highest temperature recorded during SSFSW is around the tool pin. In FSW, the force ranges from 2 to 3 kN during the advancing stage. However, in SSFSW, during the same advancing stage, the force increases significantly to a range of 15 to 20 kN. In contrast, the temperature surrounding the shoulder of the tool in SSFSW remains relatively unchanged, as the shoulder does not generate as much heat. Consequently, the material adjacent to the shoulder retains a high resistance level, leading to an increase in the force exerted on the shoulder of the tool in SSFSW.

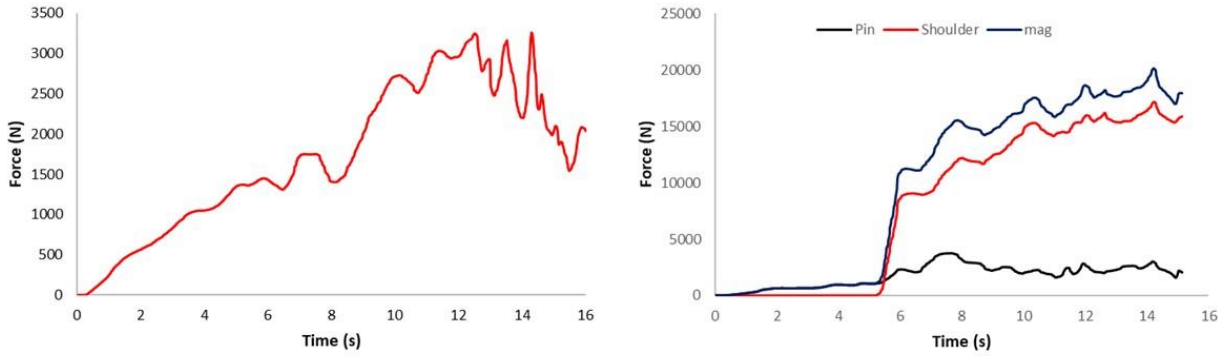

Figure 5. Comparison of axial force between FSW and SSFSW

3.3 Strain distribution in FSW and SSFSW

Within the context of FSW, strain refers to the localized deformation or distortion that occurs in the metal during the welding process. It is a physical measurement that quantifies the extent of deformation of the material.

During FSW, the rotating tool generates heat and applies pressure, causing the metal to soften and flow around the tool. Depending on the local conditions, this process leads to varying strain levels along the joint line. The metal near the front of the tool experiences high strain levels due to the intense deformation caused by the pin and shoulder.

The distribution of strain in FSW is influenced by various factors, including welding parameters, tool design, material properties, and joint geometry. Excessive strain can result in defects within the welded joint, such as cracks, voids, or residual stresses. These defects can compromise the strength and durability of the joint. Hence, it is crucial to understand and control the distribution of strain within acceptable limits during process optimization and quality assurance in FSW.

Figure 6 illustrates the variations in strain observed in cross-sectional analyses of samples welded using both FSW and SSFSW. In FSW, the affected area exhibiting strain takes on a basin-shaped pattern, as is commonly known. In SSFSW, the strain distribution is limited to the range of the tool pin. Since the tool pin used in this research is cylindrical, the area affected by strain appears as a rectangular shape in the cross-section of the sample. However, it is important to note that the shape of the affected area is entirely dependent on the shape of the tool's pin. Therefore, when a conical pin tool is utilized, the affected area will exhibit a basin shape.

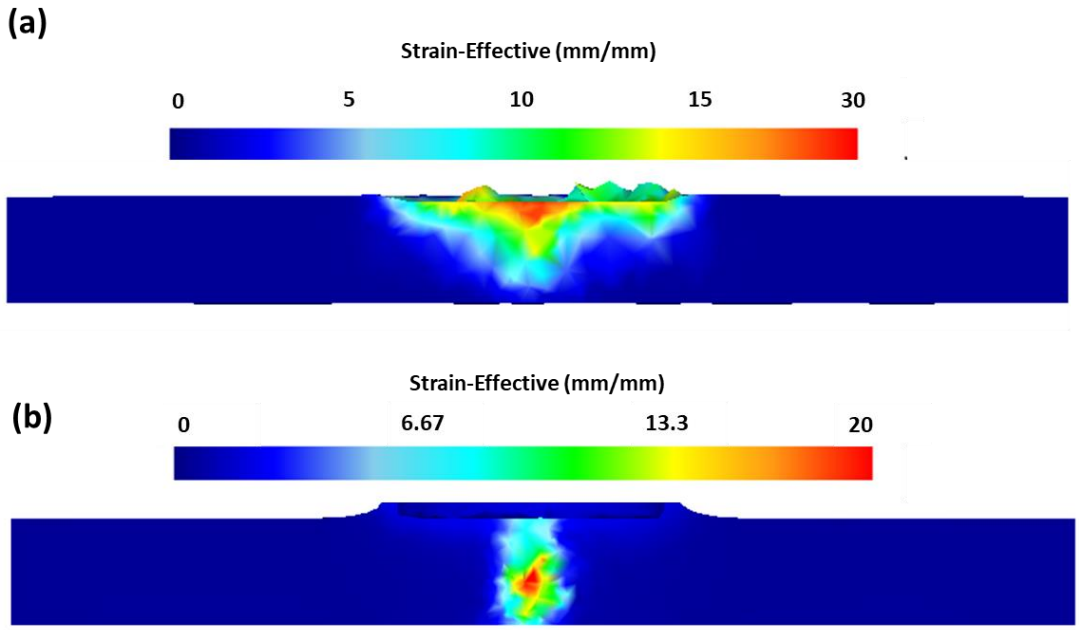

Figure 6. Strain variation of the sample produced by a) FSW b) SSTFSW

Figure 7 visually represents the cross-sectional weld morphology observed in both FSW and SSFSW joints [23]. Notably, there are notable disparities in the cross-sectional weld morphology between the FSW and SSFSW joints.

The CFSW joint exhibits a basin-shaped morphology, while the SSFSW joint demonstrates a symmetrical weld morphology with a rotating pin. This is achieved through uniform through-thickness heat input and pin-dominant material flow. The SZ in different FSW techniques is categorized into specific zones: pin-affected zone and shoulder-affected zone for CFSW, and only pin-affected zone in the absence of a rotational shoulder for SSFSW. In CFSW, the higher heat input from the weld surface results in a larger TMAZ and HAZ near the weld surface. These zones gradually reduce towards the welded bottom.

Moreover, the accuracy of a numerical prediction regarding the strain-affected area in the weld is evaluated by comparing it with experimental observations. In this case, the predicted area affected by strain from the numerical method aligns well with the experimental observations, indicating that the numerical method correctly predicts the region in the weld where the materials undergo significant strain. This agreement between the simulation prediction and experimental findings adds confidence in the model's ability to capture and predict strain distribution in the weld region accurately.

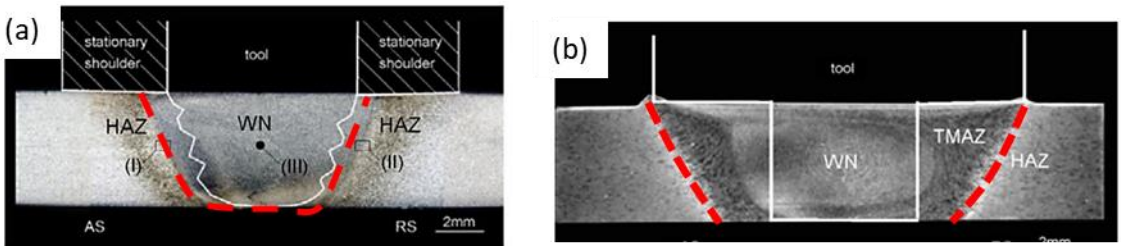

Figure 7. Cross-sectional microstructure of joints with (a) SSFSW and (b)CFSW [23]

4. Conclusion

The objective of this study was to compare various factors, including force, temperature, and strain, between CFSW and SSFSW. The following conclusions were drawn from the study:

- In CFSW, the highest temperature was observed near the surface of the samples and under the shoulder of the tool. This temperature distribution was primarily influenced by the presence of the rotating shoulder, which generated significant frictional heat. However, in SSFSW, the temperature distribution exhibited a different pattern. The highest temperature was observed in the vicinity of the rotating pin. This was attributed to the absence of a rotating shoulder in SSFSW, which played a minor role in heat generation during welding. The maximum temperature in the welding cross-section has been reduced from 350 degrees Celsius for CFSW to 200 degrees Celsius for SSFSW.
- In SSFSW, axial forces were observed on both the pin and shoulder of the tool. Initially, during the penetration stage, the force was applied solely to the pin. However, once the shoulder of the tool made contact with the workpiece, the vertical force started to increase and reached its maximum value at the end of the penetration stage. Subsequently, the axial force reduced and fluctuated within a certain range.
- The study revealed that the longitudinal forces on the tool in SSFSW were significantly higher compared to CFSW. In SSFSW, most of the axial force applied to the tool was exerted on the shoulder. Conversely, the rotational movement of the pin generated frictional heat, resulting in material softening and reduced resistance against the pin.

6. References

[1] Akbari, M., Asadi, P., Aliha, M.R.M. and Berto, F. 2023. Modeling and optimization of process parameters of the piston alloy-based composite produced by fsp using response surface methodology. Surface Review and Letters. 30(06): 2350041. doi: 10.1142/S0218625X23500415.

[2] Akbari, M., Asiabaraki, H.R. and Aliha, M.R.M. 2023. Investigation of the effect of welding and rotational speed on strain and temperature during friction stir welding of aa5083 and aa7075 using the cel approach. Engineering Research Express. 5(2): 025012. doi: 10.1088/2631-8695/acca00.

[3] Çam, G., Javaheri, V. and Heidarzadeh, A. 2023. Advances in fsw and fssw of dissimilar al-alloy plates. Journal of Adhesion Science and Technology. 37(2): 162-194. doi: 10.1080/01694243.2022.2028073.

[4] Memon, S., Fydrych, D., Fernandez, A.C., Derazkola, H.A. and Derazkola, H.A. 2021. Effects of fsw tool plunge depth on properties of an al-mg-si alloy t-joint: Thermomechanical modeling and experimental evaluation. Materials. 14(16): 4754. doi:10.3390/ma14164754.

[5] Kosturek, R., Śnieżek, L., Torzewski, J., Ślęzak, T., Wachowski, M. and Szachogłuchowicz, I. 2020. Research on the properties and low cycle fatigue of sc-modified aa2519-t62 fsw joint. Materials. 13(22): 5226. doi: 10.3390/ma13225226.

[6] Moreto, J., Dos Santos, M., Ferreira, M., Carvalho, G., Gelamo, R., Aoki, I.V., Taryba, M., Bose Filho, W.W. and Fernandes, J. 2021. Corrosion and corrosion-fatigue synergism on the base metal and nugget zone of the 2524-t3 al alloy joined by fsw process. Corrosion Science. 182: 109253. doi:10.1016/j.corsci.2021.109253.

[7] Afsari, A., Heidari, S. and Jafari, J. 2020. Evaluation of optimal conditions, microstructure, and mechanical properties of aluminum to copper joints welded by fsw. Journal of Modern Processes in Manufacturing and Production. 9(4): 61-81. doi: 20.1001.1.27170314.2020.9.4.6.4.

[8] Mohammadi Kuhbanani, H., Yasemi, H. and Aghajani Derazkola, H. 2018. Effects of tool tilt angle and plunge depth on properties of polycarbonate fsw joint. Journal of Modern Processes in Manufacturing and Production. 7(4): 41-55. doi: 20.1001.1.27170314.2018.7.4.4.8.

[9] Rezaee Hajideh, M., Farahani, M. and Khanbeigi, M.A. 2017. A hybrid thermal assisted friction stir welding approach for pmma sheets. Journal of Modern Processes in Manufacturing and Production. 6(2): 51-60. doi: 20.1001.1.27170314.2017.6.2.4.7.

[10] Sejani, D., Li, W. and Patel, V. 2022. Stationary shoulder friction stir welding–low heat input joining technique: A review in comparison with conventional fsw and bobbin tool fsw. Critical Reviews in Solid State and Materials Sciences. 47(6): 865-914. doi:10.1080/10408436.2021.1935724.

[11] Chen, Y., Li, H., Wang, X., Ding, H. and Zhang, F. 2019. A comparative investigation on conventional and stationary shoulder friction stir welding of al-7075 butt-lap structure. Metals. 9(12): 1264. doi:10.3390/met9121264.

[12] Patel, V., Li, W. and Xu, Y. 2019. Stationary shoulder tool in friction stir processing: A novel low heat input tooling system for magnesium alloy. Materials and manufacturing processes. 34(2): 177-182. doi:10.1080/10426914.2018.1544716.

[13] Akbari, M., Asadi, P. and Sadowski, T. 2023. A review on friction stir welding/processing: Numerical modeling. Materials. 16(17): 5890. doi:10.3390/ma16175890.

[14] R, S.R., Jagadish, Rao, C.J., Kumar Aadapa, S. and Yanda, S. 2022. Predication of temperature distribution and strain during fsw of dissimilar aluminum alloys using deform 3d. Materials Today: Proceedings. 59: 1760-1767. doi:10.1016/j.matpr.2022.04.371.

[15] Akbari, M., Rahimi Asiabaraki, H., Hassanzadeh, E. and Esfandiar, M. 2023. Simulation of dissimilar friction stir welding of aa7075 and aa5083 aluminium alloys using coupled eulerian–lagrangian approach. Welding International. 37(4): 174-184. doi:10.1080/09507116.2023.2205035.

[16] Akbari, M., Aliha, M.R.M. and Berto, F. 2023. Investigating the role of different components of friction stir welding tools on the generated heat and strain. Forces in Mechanics. 10: 100166. doi:10.1016/j.finmec.2023.100166.

[17] Asadi, P., Mahdavinejad, R.A. and Tutunchilar, S. 2011. Simulation and experimental investigation of fsp of az91 magnesium alloy. Materials Science and Engineering: A. 528(21): 6469-6477. doi:10.1016/j.msea.2011.05.035.

[18] Buffa, G., Ducato, A. and Fratini, L. 2013. Fem based prediction of phase transformations during friction stir welding of ti6al4v titanium alloy. Materials Science and Engineering: A. 581(0): 56-65. doi:10.1016/j.msea.2013.06.009.

[19] Akbari, M., Aliha, M., Keshavarz, S. and Bonyadi, A. 2019. Effect of tool parameters on mechanical properties, temperature, and force generation during fsw. Proceedings of the Institution of Mechanical Engineers, Part L: Journal of Materials: Design and Applications. 233(6): 1033-1043. doi:10.1177/1464420716681591.

[20] Terra, C.S. and Silveira, J.L.L. 2021. Models for fsw forces using a square pin profile tool. Journal of Manufacturing Processes. 68: 1395-1404. doi:10.1016/j.jmapro.2021.06.052

[21] Khan, N.Z., Bajaj, D., Siddiquee, A.N., Khan, Z.A., Abidi, M.H., Umer, U. and Alkhalefah, H. 2019. Investigation on effect of strain rate and heat generation on traverse force in fsw of dissimilar aerospace grade aluminium alloys. Materials. 12(10): 1641. doi:10.3390/ma12101641.

[22] Jaffarullah, M.S., Low, C.Y., Shaari, M.S.B. and Jaffar, A. 2015. A review of force control techniques in friction stir process. Procedia Computer Science. 76: 528-533. doi:10.1016/j.procs.2015.12.331.

[23] Li, D., Yang, X., Cui, L., He, F. and Shen, H. 2014. Effect of welding parameters on microstructure and mechanical properties of aa6061-t6 butt welded joints by stationary shoulder friction stir welding. Materials & Design. 64: 251-260. doi:10.1016/j.matdes.2014.07.046.